

Electrolyte-Phobic Surface for the Next-Generation Nanostructured Battery Electrodes

Chenxi Qian, Jie Zhao, Yongming Sun,* Hye Ryoung Lee, Langli Luo, Meysam Makaremi, Sankha Mukherjee, Jiangyan Wang, Chenxi Zu, Meikun Xia, Chongmin Wang, Chandra Veer Singh,* Yi Cui,* and Geoffrey A. Ozin*



Cite This: *Nano Lett.* 2020, 20, 7455–7462



Read Online

ACCESS |



Metrics & More



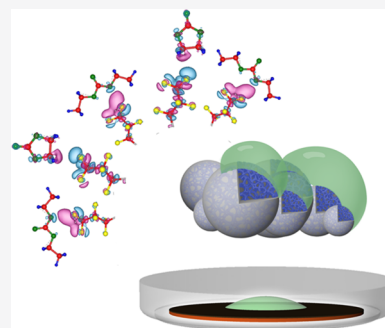
Article Recommendations



Supporting Information

ABSTRACT: Nanostructured electrodes are among the most important candidates for high-capacity battery chemistry. However, the high surface area they possess causes serious issues. First, it would decrease the Coulombic efficiencies. Second, they have significant intakes of liquid electrolytes, which reduce the energy density and increase the battery cost. Third, solid-electrolyte interphase growth is accelerated, affecting the cycling stability. Therefore, the interphase chemistry regarding electrolyte contact is crucial, which was rarely studied. Here, we present a completely new strategy of limiting effective surface area by introducing an “electrolyte-phobic surface”. Using this method, the electrolyte intake was limited. The initial Coulombic efficiencies were increased up to ~88%, compared to ~60% of the control. The electrolyte-phobic layer of Si particles is also compatible with the binder, stabilizing the electrode for long-term cycling. This study advances the understanding of interphase chemistry, and the introduction of the universal concept of electrolyte-phobicity benefits the next-generation battery designs.

KEYWORDS: battery solid-electrolyte interphase (SEI), surface chemistry, electrolyte-phobicity, perfluorocarbon coating



Nanostructured electrodes, innovatively and rationally designed to enable high capacity battery chemistry, are holding great promise and substantial significance today.^{1–14} Nanostructures are able to resolve the volume change and mechanical fragmentation issues that high-capacity battery materials suffer. However, they present high surface area and high reaction activity, which poses final obstacles for the real-world applications of these electrodes in batteries, that is, (1) the high surface area of nanomaterials causes a large amount of liquid electrolyte intake at the electrode level, which reduces the overall energy density and increases the cost of the battery; (2) coulombic efficiencies drop significantly, since the side chemical reactions scale with surface area and reaction activity;¹⁵ and (3) the formation and growth of solid-electrolyte interphase (SEI) layers are accelerated, affecting the cycling stability and battery performance. In the past, there have been attempts to use a coating layer on secondary particles¹⁶ to reduce surface area. Here, we present a completely new idea of limiting effective surface area by controlling the wetting behavior of the electrolyte.

To demonstrate this strategy, we choose Si as the model material. Si has 10 times the theoretical specific capacity of traditional graphite anodes. However, the large volume expansion of Si during battery operation poses a major challenge, causing complications such as mechanical fracture, loss of interparticle electrical contact, and recurring side reactions with the electrolyte. Researchers have been urged to

develop a variety of innovative material designs.^{7,14,17–21} Utilizing these nanostructures is a useful strategy to buffer the volume expansion of Si during lithiation.²² However, nanoporous Si anodes reported to date suffer from low first-cycle Coulombic efficiencies,²² because of the large intrinsic surface area and high reaction activity of the nanoporous structure. The absorption of a large amount of liquid electrolytes by the porous structure also reduces the overall energy density and increases the cost of the battery. Therefore, a new strategy allowing minimum electrolyte infiltration, while maintaining maximum performance, is a key requirement for a new generation of porous Si nanostructures.

Herein, we introduce the universal concept of an “electrolyte-phobic surface” to address the problems seen in high-surface-area nanostructured materials. Electrolyte-phobic surfaces reduce the effective surface area, leaving the interior void space unaffected and bringing minimum changes to the structure itself. The intake of electrolyte was thus controlled at a low level. The designed electrolyte-phobic sample in practice

Received: July 12, 2020

Revised: September 28, 2020

Published: October 5, 2020



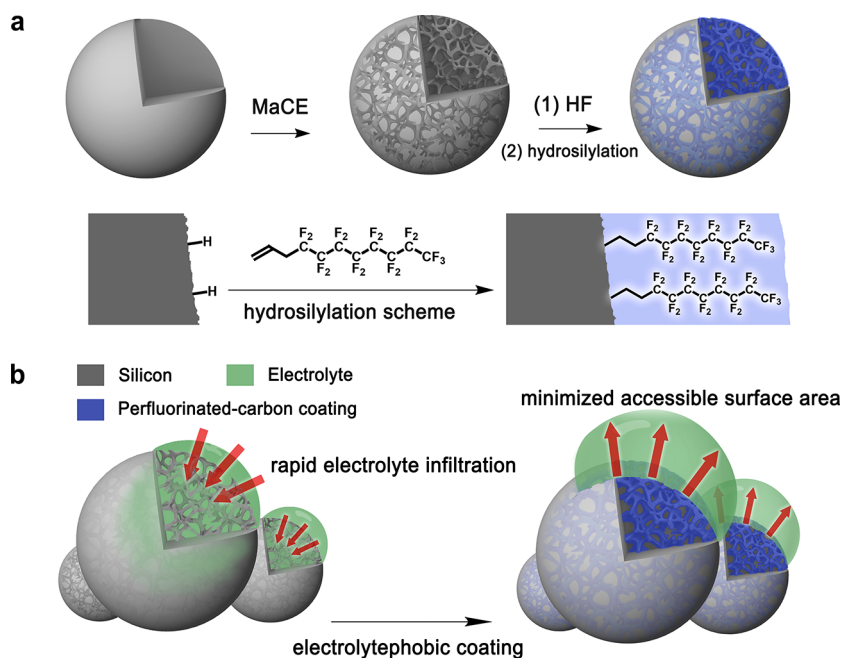


Figure 1. Design and structure of the pSi:PFD. (a) The reaction schemes for preparing porous silicon nanoparticles by MaCE and subsequent surface treatment by hydrosilylation. (b) Design strategy: In the case of pristine porous silicon nanoparticles, there is rapid electrolyte infiltration and SEI formation during battery operations.

achieved an 88% initial Coulombic efficiency compared to the control sample without the electrolyte-phobic property, which showed a mere 60% efficiency under the same conditions. With enhanced van der Waals interactions^{23–33} between the PVDF binder and silicon, the covalently linked surface coating promotes great robustness of the electrode when using the conventional PVDF binders. The cycling stability would therefore be enhanced.

RESULTS AND DISCUSSION

Materials Design and Characterization. We prepared porous silicon via a metal-assisted chemical etching (MaCE) method^{34,35} on silicon submicron-particles with a mean size of 800 nm. Previous reports showed that the critical fracture sizes of crystalline Si are around 240–400 nm for nanopillars and nanowires³⁶ or 150 nm for nanoparticles.³⁷ After the MaCE process, these porous silicon (pSi) particles kept their original size but their inner structures became porous (Figure 1a). The void space in the porous structure (Figures 2b and S2) offers the silicon walls an opportunity to readily expand and contract.

In order to achieve an electrolyte-phobic surface, the pSi submicron-particles were treated with hydrosilylation by 1H,1H,2H-perfluoro-1-decene (PFD) (Figure 1a), covalently linking PFD chains onto the pSi surface.³⁸ Fourier-transform infrared (FTIR) spectrum (Figure S1), energy-dispersive X-ray (EDX) mapping (Figure S3 and Figure 2c–f), and X-ray photoelectron spectroscopy (XPS) spectra (Figure 2g–i) of the perfluorocarbon-coated porous silicon nanoparticles (pSi:PFD) show there is successful covalent and uniform coating on the surface. The coating layer was firm and resistant to moderate physical friction due to the silicon–carbon covalent bonds. After coating, the porous structure of the particle was not compromised (Figure 2b and Figure S4). We expect minimized electrolyte infiltration when these pSi:PFD particles were immersed in electrolytes (Figure 1b). TEM images of the

pSi:PFD samples show surface/void space coverage by the amorphous organic material.³⁹

Battery Testing, Mechanism, and Proof-of-Concept Studies. Coin cells with metallic lithium counter electrodes were fabricated to evaluate the electrochemical performance (see Supporting Information, Materials and Methods, for details). Figure 3c–f shows the half-cell data. For the first three cycles, at a current density of C/20 ($1C = 4.2 \text{ A g}^{-1}$) the reversible capacity of both pSi:PFD and the control sample, pSi, were up to $\sim 3800 \text{ mAh g}^{-1} \text{ Si}$, only 10% less than the theoretical capacity of Si anodes ($4200 \text{ mAh g}^{-1} \text{ Si}$).

Such high capacities dispel doubts whether the porous structure internally would maintain an electrically connected status. From the performance and normal cycling profile (Figure 3d and Figure S6) of the pSi:PFD-based anodes, another doubt would be dispelled whether the electrolyte-phobic surface coverage of perfluorocarbon chains could hinder the lithiation and delithiation process. The stacked perfluorocarbon chains likely offer lithium migrating channels so that lithium ions can easily pass through them.

For the later cycles (the fourth and thereafter), continued cycling at a higher rate of C/2 was employed. Figure 3c shows that the capacity of pSi quickly decreased to $\sim 200 \text{ mAh g}^{-1}$ as early as ~ 30 cycles and remained this low value thereafter. In dramatic contrast, the capacity of pSi:PFD is seen to remain at 2000 mAh g^{-1} at 60 cycles and 1750 mAh g^{-1} at 100 cycles. Although further work is needed to meet the commercial standard, the pSi:PFD materials have a far more superior capacity retention than the pristine pSi.

In a practical battery, cycling stability is not the only important merit. High Coulombic efficiencies (especially early cycle) are equally crucial. A lower early cycle Coulombic efficiency denotes a greater Li-ion loss and electrolyte consumption during SEI formation. For porous silicon, the high surface area of the porous structure induces more side reactions, resulting in fast and continuous SEI formation and lowered Coulombic efficiencies.

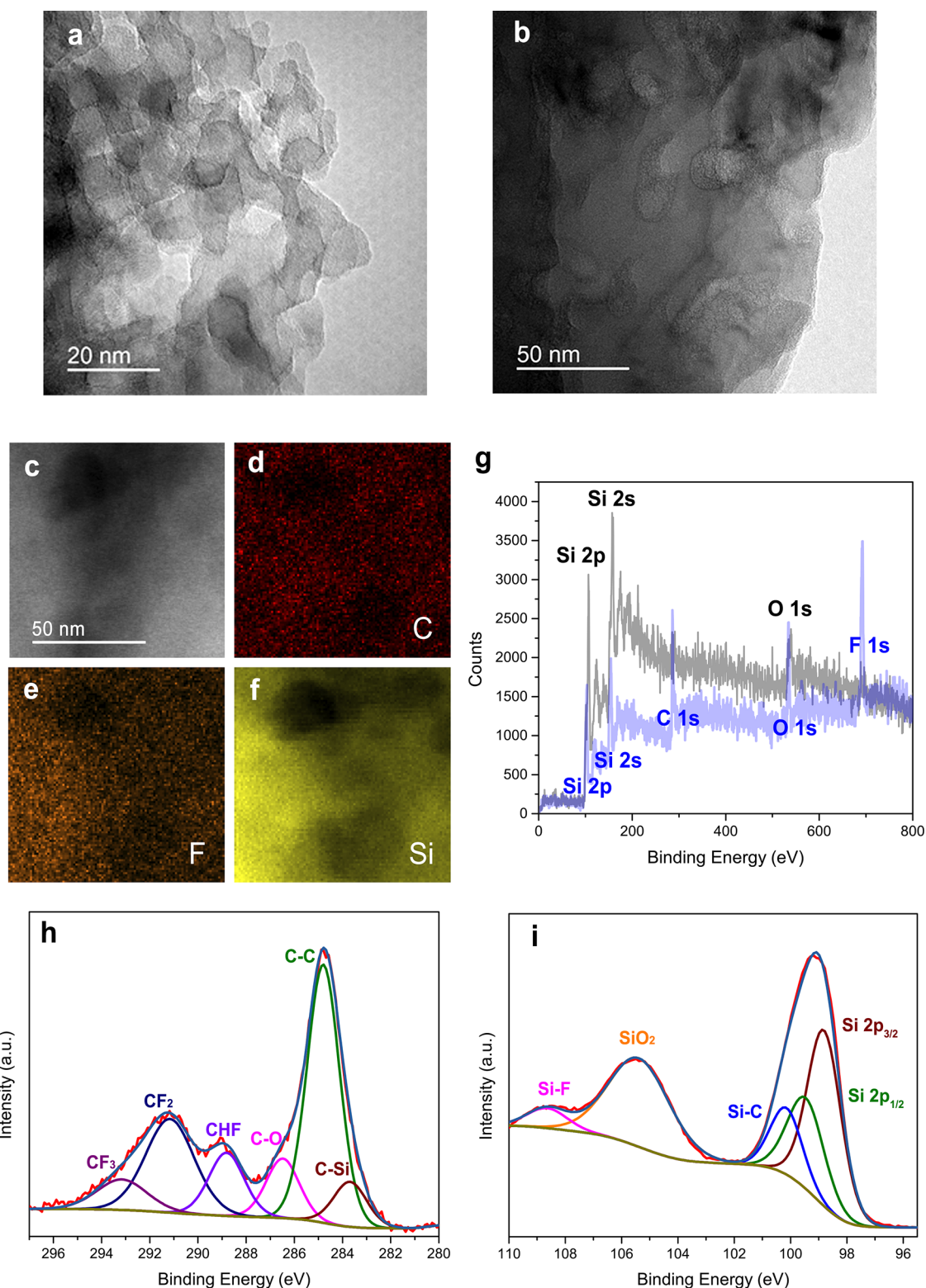


Figure 2. Materials characterization. (a) A typical TEM image of a single porous silicon particle (scale bar: 20 nm). The internal void space of the porous silicon particle is distinct. (b) TEM image of a pSi:PFD where the pores are seen to be filled with soft, amorphous carbon material. (c–f) EDX mapping of the pSi:PFD particle. (g) XPS survey scan of the pristine porous silicon particles (pSi, in black) and the pSi:PFD (in blue). (h,i) High-resolution XPS spectra of carbon 1s peaks and silicon 2p peaks.

What we emphasize here is the improvement in early cycle Coulombic efficiencies of pSi:PFD. As shown in Figure 3e, pSi:PFD has a significantly higher first-cycle Coulombic efficiency up to 88%, while pSi has ~60%. In later cycles, the

Coulombic efficiency of pSi:PFD and pSi increased to 99.3% and 99.8%, respectively. As a reference, the first-cycle Coulombic efficiency in commercial graphite anodes is 90–94%, increasing to 99.9% in later cycles.⁴⁰ We attribute the

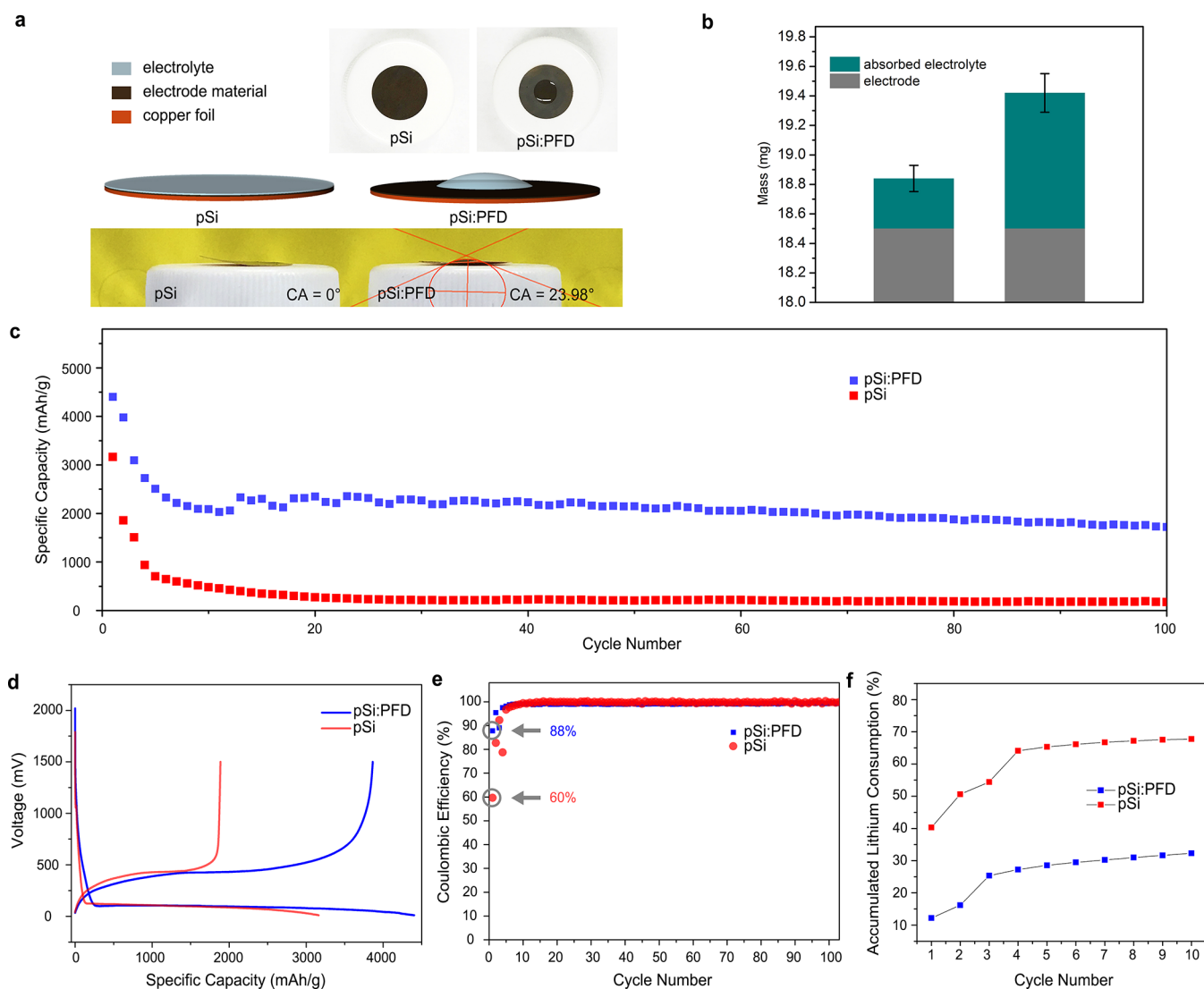


Figure 3. Battery fabrication and testing. (a) Different wetting behavior of electrodes made from pSi:PFD and the pristine pSi. (b) A comparison between the mass of absorbed electrolytes on different electrodes (error bars based on of five parallel measurements). (c) Reversible delithiation capacity for the first 100 galvanostatic cycles of pSi:PFD and the pristine pSi. (d) Voltage profiles of the pSi:PFD and pSi plotted for the first cycles. The first two cycles of both samples are plotted in Figure S6. (e) Coulombic efficiencies of the first 100 cycles for pSi:PFD and the pristine pSi. (f) Accumulated lithium consumption for pSi:PFD and the pristine pSi for the first 10 cycles.

greatly enhanced initial Coulombic efficiencies of pSi:PFD to the unique wetting behavior of such a porous structure. The electrolyte-phobic nature of the electrode materials lowers the accessible surface area and minimizes side reactions significantly. Meanwhile, the internal porous structure still allows the silicon walls to expand and contract instead of cracking. This guarantees the cycling stability in these tests. On the other hand, the pristine pSi structure has a greater tendency to break and fail owing to the uncontrolled SEI formation on the internal surface, which accounts for its poor cycling stability. A comparison between the accumulated lithium consumption during cycling (Figure 3f) showed pSi lost more lithium during the first 10 cycles.

To demonstrate the electrolyte-phobicity of our sample, the same batches of electrodes made from pSi:PFD and pSi employed for the battery testing were used in the following experiment. The electrolyte solution with the exact composition in the battery testing was set onto the horizontally placed electrode surface. The electrolyte droplet on pSi:PFD electrode surface showed distinct curvature and the contact angle was

measured at 23.98° (Figure 3a). In contrast, the pSi electrode surface favored a complete wetting of the electrolyte droplet. Apparently the pSi:PFD electrode surface was electrolyte-phobic while the control was electrolyte-philic, which proves our hypothesis that the effective surface area accessible by the electrolyte is minimized in the case of pSi:PFD.

Another quantifiable demonstration of wetting employed a common drop-casting method. After quickly removing the electrolyte above the electrode surface, we were able to weigh the electrode with absorbed electrolyte (Figure 3b). The same amount of active materials after absorbing electrolyte weighed noticeably different. The pSi:PFD electrode absorbed 0.36 ± 0.11 mg of electrolyte while the pSi electrode absorbed 0.92 ± 0.13 mg.

Apart from the electrode-level demonstration of the electrolyte-phobic property, we did a simple particle-level study using optical microscopy (Figure S5). When immersed in the same electrolyte, the color of pSi:PFD particles appeared lighter and the color of pSi particles appeared darker. This is due to pSi

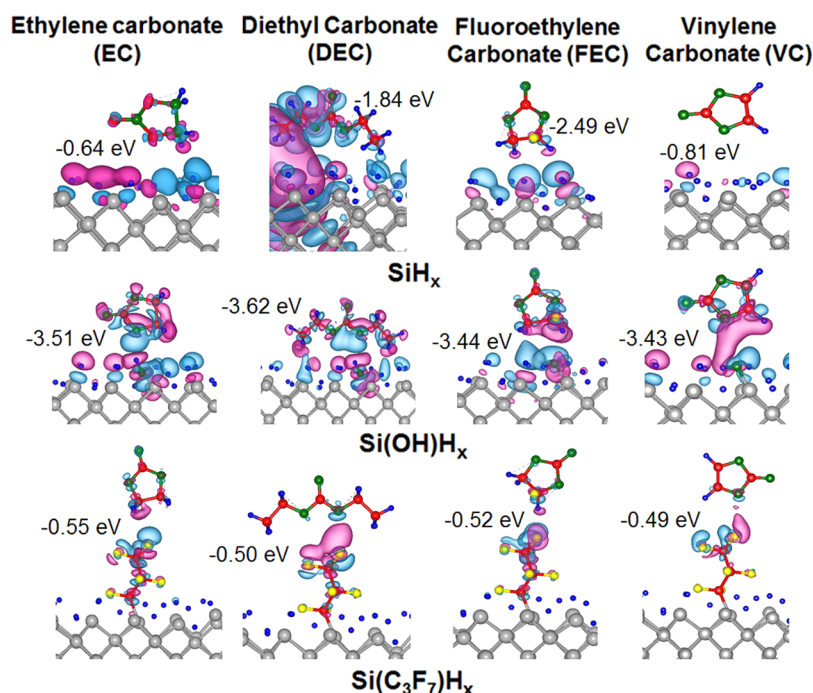


Figure 4. DFT simulation results: Charge density difference plots of the stable adsorption of ethyl carbonate, diethyl carbonate, fluoroethylene carbonate, and vinylene carbonate over all-hydride terminated (SiH_x), hydroxide-terminated (Si(OH)_{x-1}), and fluorocarbon-chain-terminated ($\text{Si(C}_3\text{F}_7)_x$) Si surfaces. Color code for atoms: gray, Si; red, C; blue, H; yellow, F; and green, O. The isosurface level is set to be $0.00025 \text{ e}\text{\AA}^{-3}$, blue and pink isosurfaces indicate charge accumulation and depletion, respectively.

particles absorbing electrolyte while pSi:PFD particles did not. These light scattering differences were derived from the refractive index change when liquid fills the void space where there was trapped air originally.

Conveniently, the cycling stability benefits not only from the electrolyte-phobic nature of pSi:PFD electrodes but also from the binder effect. As illustrated in Figure S7, with perfluorocarbon coating the pSi:PFD surface possesses enhanced van der Waals (VDW) interactions with the PVDF binder. This adds to the robustness of the electrode, making it more resistant to electrode-level degradation during cycling. We demonstrated this effect with microscopy studies. The copper electrodes calendared with active materials, as used in actual battery cycling tests, exhibited different extensibilities and robustness when exposed to the same stress. We bent the electrodes to a certain angle (101°). Under SEM, the pSi-based electrode showed fracture at this bent angle whereas the pSi:PFD based electrode was intact (Figure S8). With enhanced VDW interactions between PVDF and perfluorocarbon surface, the particles are held together much more strongly. This revelation inspires opportunities for battery development employing Si anodes without binder. The perfluorocarbon surface could act as PVDF and bind the particles together. The envisioned benefits of binder-free anodes would be enormous. First, there is greatly enhanced electrical conductivity. Second, to be free of PVDF means less electrochemically inactive material, which leads to a higher capacity. Third, less carbon additive would be needed.

In order to further confirm that the electrolyte-phobic surface minimized electrolyte infiltration and prevented fast SEI formation in initial cycles, we did XPS studies on the pSi:PFD electrode *ex situ* following battery operations. The XPS spectra collected after one cycle exhibited evidence for a dominant surface species of perfluorocarbon molecules, but a negligible amount of SEI components by comparison (Figure S11). In the

later cycles, the lithium consumption of both electrodes reached a similar and very low level (Figure S12), proving that the initial cycles were crucial to the battery performance in general (considering the drastic difference in their corresponding cycling performance shown in Figure 3).

DFT Simulations. In addition to the macroscopic (electrode-level and particle-level) studies, it is important to delve deeper and evaluate on the molecular level. Therefore, we performed density functional theory (DFT) simulations to probe different binding modes and to evaluate the corresponding binding energies of each constituent molecule of the electrolyte on the surface sites of pSi:PFD and pSi. VDW forces were taken into account by utilizing a dispersion corrected approach (DFT+D2)^{41,42} (see Supporting Information, Materials and Methods, for details).

Stronger interactions would contribute to a more wettable surface. According to the binding energy values in Figure 4, the electrolyte molecules bind more strongly to the pristine surfaces than the perfluorocarbon-chain-terminated surface. Moreover, high energy substrates (the pristine silicon substrates) are more easily wet than low energy substrates (the perfluorocarbon-chain-terminated surface).⁴³ The electrolyte droplet is a molecular liquid with a relative low surface tension. Therefore, when the droplet was set onto a high-energy surface, the inevitable outcome is complete wetting. The capillary motion would also facilitate the wetting process. While on the treated substrate, the packed perfluorocarbon chains are held by weak VDW force. Extremely weak VDW interactions with the solvent molecules stem from the low density of interaction sites, which can be estimated with a standard self-assembled monolayer (SAM) model.⁴⁴ The hydrophobicity from this origin is anticipated not only for water but also for polar liquids with high cohesive energies. The solvent carbonate molecules used here (EC, DEC, FEC, and VC) have high cohesive energies,

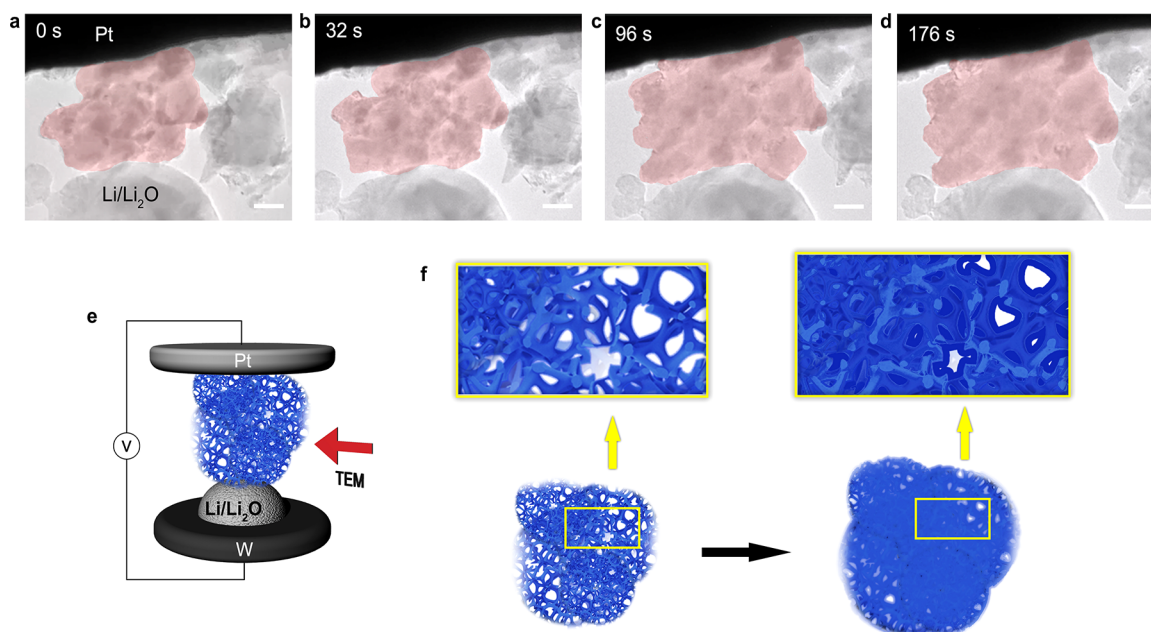


Figure 5. *In situ* TEM characterization of the perfluorocarbon-coated porous silicon particle during lithiation. (a–d) Lithiation of a perfluorocarbon coated porous silicon particle (scale bar: 400 nm). (e) Schematic of the *in situ* TEM electrochemical cell used in this study. (f) Schematic of the volume expansion of Si within the porous structure.

benefiting from their large permanent dipoles.⁴⁵ Therefore, the surface is expected to undergo partial wetting for the electrolyte solvents, rather than complete wetting. On the molecular and soft bulk materials level, both factors guarantee that the treated surface is not as wettable as the pristine surface.

***In Situ* TEM Study.** During lithiation and cycling of conventional silicon particle-based anodes, the volume expansion of Si would lead to electrode particle fracture, disconnection between particles, and finally capacity loss and limited cycle life. To demonstrate the lithiation process of the pSi:PFD particle *in situ*, we used a nanoscale electrochemical cell inside the TEM (as shown in the scheme in Figure 5e).^{46,47} These experiments open a window for us to observe directly silicon's intrinsic volume expansion during battery cycling and to observe if there is particle level fracture. From Figure 5a–d and Supporting Information Video 1, we could see the pSi:PFD particle expanded moderately and did not show fracture during the whole lithiation process. This observation indicates that the internal void space is being occupied in the lithiation process by the expanding silicon, as shown by the schematic in Figure 5f. It is worth noting that we observed in the lithiation/expansion process that the original particle remained as a whole and retained its electrical contact internally. The porous structure and uniformly distributed void space significantly helped dissipate the interior stress caused by the volume expansion. In previous reports on the *in situ* observation of nonporous Si nanoparticle or microparticle lithiation, these particles showed clear cracks, quite distinct from what we observed in the case of pSi:PFD.³⁷ In addition, multiple particles were observed to stick to each other during the lithiation process. The large particle aggregate (in red in Figure 5a–d) did not disintegrate even without the presence of a binder, which is due to the enhanced surface interactions between coated pSi:PFD particles. This observation further supports our argument in previous discussions that the perfluorocarbon coating helps to improve the electrode-level robustness, contributing to the long-term cycling stability.

CONCLUSION

Our strategy, described for the first time herein, has solved a long-standing problem that has perplexed researchers: the complications caused by the high surface area of nanostructured electrodes. Specifically, we established a facile synthetic approach to coat the surface of the active material with a chemically tethered perfluorocarbon that provides it with a unique nonwetting behavior making it impervious to the electrolyte. This innovative design reduces the accessible surface area of the active material in nanostructured anodes, minimizes side reactions during SEI formation, enhances the initial Coulombic efficiencies, improves the cycling stability, and limits the electrolyte intake to a low level.

Moreover, this surface design strategy achieves compatibility of the Si surface with the conventional PVDF binder, enhancing the electrode-level stability during cycling.

Through precise tuning of the synthesis–structure–property relationships, we have significantly improved all performance metrics. We envision the concept of electrolyte-phobic perfluorocarbon coatings could prove to be a general strategy for minimizing the accessible surface area of high-surface-area materials in future applications in advanced batteries.

ASSOCIATED CONTENT

Supporting Information

The Supporting Information is available free of charge at <https://pubs.acs.org/doi/10.1021/acs.nanolett.0c02880>.

Materials and methods, including synthesis of porous Si nanoparticles with perfluorinated-carbon electrolyte-phobic layer, battery fabrication, DFT simulations, and *in situ* TEM study (PDF)

In situ TEM observation of morphological evolution of pSi:PFD particle when negatively biasing the working electrode to make Li⁺ ions flow through the oxide layer and be reduced at the working electrode, where they alloy with Si (MP4)

■ AUTHOR INFORMATION

Corresponding Authors

Yongming Sun – Wuhan National Laboratory for Optoelectronics, Huazhong University of Science and Technology, Wuhan 430074, China; orcid.org/0000-0001-8528-525X; Email: yongmingsun@hust.edu.cn

Chandra Veer Singh – Department of Materials Science and Engineering, University of Toronto, Toronto, Ontario M5S 3E4, Canada; orcid.org/0000-0002-6644-0178; Email: chandraveer.singh@utoronto.ca

Yi Cui – Department of Materials Science and Engineering, Stanford University, Stanford, California 94305, United States; Stanford Institute for Materials and Energy Sciences, SLAC National Accelerator Laboratory, Menlo Park, California 94025, United States; orcid.org/0000-0002-6103-6352; Email: yicui@stanford.edu

Geoffrey A. Ozin – Department of Chemistry, University of Toronto, Toronto, Ontario M5S 3H6, Canada; orcid.org/0000-0002-6315-0925; Email: gozin@chem.utoronto.ca

Authors

Chenxi Qian – Department of Materials Science and Engineering, Stanford University, Stanford, California 94305, United States; Department of Chemistry, University of Toronto, Toronto, Ontario M5S 3H6, Canada

Jie Zhao – Department of Materials Science and Engineering, Stanford University, Stanford, California 94305, United States; orcid.org/0000-0001-6446-8313

Hye Ryoung Lee – Department of Materials Science and Engineering, Stanford University, Stanford, California 94305, United States

Langli Luo – Institute of Molecular Plus, Tianjin Key Laboratory of Molecular Optoelectronic Sciences, Department of Chemistry, Tianjin University, Tianjin 300072, China; orcid.org/0000-0002-6311-051X

Meysam Makaremi – Department of Materials Science and Engineering, University of Toronto, Toronto, Ontario M5S 3E4, Canada

Sankha Mukherjee – Department of Materials Science and Engineering, University of Toronto, Toronto, Ontario M5S 3E4, Canada; orcid.org/0000-0001-9094-0538

Jiangyan Wang – Department of Materials Science and Engineering, Stanford University, Stanford, California 94305, United States; Stanford Institute for Materials and Energy Sciences, SLAC National Accelerator Laboratory, Menlo Park, California 94025, United States; orcid.org/0000-0001-6951-1296

Chenxi Zu – Department of Materials Science and Engineering, Stanford University, Stanford, California 94305, United States

Meikun Xia – Department of Chemistry, University of Toronto, Toronto, Ontario M5S 3H6, Canada

Chongmin Wang – Environmental Molecular Sciences Laboratory, Pacific Northwest National Laboratory, Richland, Washington 99352, United States; orcid.org/0000-0003-3327-0958

Complete contact information is available at: <https://pubs.acs.org/10.1021/acs.nanolett.0c02880>

Notes

The authors declare no competing financial interest.

■ ACKNOWLEDGMENTS

G.A.O. is deeply grateful to the Natural Sciences and Engineering Research Council of Canada (NSERC) for the strong and sustained support of his materials chemistry and nanochemistry research. Y.C. acknowledges support from the Assistant Secretary for Energy Efficiency and Renewable Energy, Office of Vehicle Technologies of the U.S. Department of Energy, under the Battery Materials Research (BMR) program. C.Q. acknowledges the Connaught Fund and Department of Chemistry at the University of Toronto for funding. C.Q. also would like to thank T. B. Schon and D. S. Seferos for access to their battery assembly facility in Toronto.

■ REFERENCES

- (1) Armand, M.; Tarascon, J.-M. Building better batteries. *Nature* **2008**, *451*, 652–657.
- (2) Sun, Y.; Liu, N.; Cui, Y. Promises and challenges of nanomaterials for lithium-based rechargeable batteries. *Nat. Energy* **2016**, *1*, 16071.
- (3) Aricò, A. S.; Bruce, P.; Scrosati, B.; Tarascon, J.-M.; van Schalkwijk, W. Nanostructured materials for advanced energy conversion and storage devices. *Nat. Mater.* **2005**, *4*, 366–377.
- (4) Li, H.; Wang, Z.; Chen, L.; Huang, X. Research on advanced materials for Li-ion batteries. *Adv. Mater.* **2009**, *21*, 4593–4607.
- (5) Fang, Y.; Yu, X.-Y.; Lou, X. W. D. Nanostructured Electrode Materials for Advanced Sodium-Ion Batteries. *Matter* **2019**, *1*, 90–114.
- (6) Bruce, P. G.; Freunberger, S. a.; Hardwick, L. J.; Tarascon, J.-M. Li–O₂ and Li–S batteries with high energy storage. *Nat. Mater.* **2012**, *11*, 19–29.
- (7) Chan, C.; et al. High-performance lithium battery anodes using silicon nanowires. *Nat. Nanotechnol.* **2008**, *3*, 31–35.
- (8) Ji, X.; Lee, K. T.; Nazar, L. F. A highly ordered nanostructured carbon–sulphur cathode for lithium–sulphur batteries. *Nat. Mater.* **2009**, *8*, 500–506.
- (9) Wang, J.; Cui, Y.; Wang, D. Design of Hollow Nanostructures for Energy Storage, Conversion and Production. *Adv. Mater.* **2019**, *31*, 1801993.
- (10) Qian, J.; et al. High rate and stable cycling of lithium metal anode. *Nat. Commun.* **2015**, *6*, 6362.
- (11) Zheng, G.; et al. Interconnected hollow carbon nanospheres for stable lithium metal anodes. *Nat. Nanotechnol.* **2014**, *9*, 618–623.
- (12) Yang, S.; Zavalij, P. Y.; Whittingham, M. S. Anodes for lithium batteries: Tin revisited. *Electrochem. Commun.* **2003**, *5*, 587–590.
- (13) Wei Seh, Z.; Li, W.; Cha, J. J.; Zheng, G.; Yang, Y.; McDowell, M. T.; Hsu, P.-C.; Cui, Y. Sulphur–TiO₂ yolk–shell nanoarchitecture with internal void space for long-cycle lithium–sulphur batteries. *Nat. Commun.* **2013**, *4*, 1331.
- (14) Magasinski, A.; et al. High-performance lithium-ion anodes using a hierarchical bottom-up approach. *Nat. Mater.* **2010**, *9*, 461–461a.
- (15) Pinson, M. B.; Bazant, M. Z. Theory of SEI Formation in Rechargeable Batteries: Capacity Fade, Accelerated Aging and Lifetime Prediction. *J. Electrochem. Soc.* **2013**, *160*, A243.
- (16) Liu, N.; et al. A pomegranate-inspired nanoscale design for large-volume-change lithium battery anodes. *Nat. Nanotechnol.* **2014**, *9*, 187–192.
- (17) Liu, N.; et al. A yolk-shell design for stabilized and scalable Li-ion battery alloy anodes. *Nano Lett.* **2012**, *12*, 3315–3321.
- (18) Li, Y.; Yan, K.; Lee, H.-W.; Lu, Z.; Liu, N.; Cui, Y. Growth of conformal graphene cages on micrometre-sized silicon particles as stable battery anodes. *Nat. Energy* **2016**, *1*, 15029.
- (19) Ge, M.; Rong, J.; Fang, X.; Zhou, C. Porous doped silicon nanowires for lithium ion battery anode with long cycle life. *Nano Lett.* **2012**, *12*, 2318–2323.
- (20) Xiao, J.; et al. Stabilization of Silicon Anode for Li-Ion Batteries. *J. Electrochem. Soc.* **2010**, *157*, A1047.
- (21) Li, X.; Gu, M.; Hu, S.; Kennard, R.; Yan, P.; Chen, X.; Wang, C.; Sailor, M. J.; Zhang, J.-G.; Liu, J. Mesoporous silicon sponge as an anti-

pulverization structure for high-performance lithium-ion battery anodes. *Nat. Commun.* **2014**, *5*, 4105.

(22) Lu, Z.; et al. Non filling Carbon Coating of Porous Silicon Micrometer-Sized Particles for High-Performance. *ACS Nano* **2015**, *9*, 2540–2547.

(23) Jeong, Y. K.; et al. Millipede-inspired structural design principle for high performance polysaccharide binders in silicon anodes. *Energy Environ. Sci.* **2015**, *8*, 1224–1230.

(24) Murase, M.; et al. Crop-derived polysaccharides as binders for high-capacity silicon/graphite-based electrodes in lithium-ion batteries. *ChemSusChem* **2012**, *5*, 2307–2311.

(25) Salem, N.; Lavrisa, M.; Abu-Lebdeh, Y. Ionically-Functionalized Poly(thiophene) Conductive Polymers as Binders for Silicon and Graphite Anodes for Li-Ion Batteries. *Energy Technol.* **2016**, *4*, 331–340.

(26) Kwon, T. W.; et al. Dynamic Cross-Linking of Polymeric Binders Based on Host-Guest Interactions for Silicon Anodes in Lithium Ion Batteries. *ACS Nano* **2015**, *9*, 11317–11324.

(27) Zhao, H.; et al. Conductive polymer binder for high-tap-density nanosilicon material for lithium-ion battery negative electrode application. *Nano Lett.* **2015**, *15*, 7927–7932.

(28) Kwon, T. W.; et al. Systematic molecular-level design of binders incorporating Meldrum's acid for silicon anodes in lithium rechargeable batteries. *Adv. Mater.* **2014**, *26*, 7979–7985.

(29) Han, Z.-J.; Yabuuchi, N.; Hashimoto, S.; Sasaki, T.; Komaba, S. Cross-Linked Poly(acrylic acid) with Polycarbodiimide as Advanced Binder for Si/Graphite Composite Negative Electrodes in Li-Ion Batteries. *ECS Electrochem. Lett.* **2013**, *2*, A17–A20.

(30) Koo, B.; et al. A highly cross-linked polymeric binder for high-performance silicon negative electrodes in lithium ion batteries. *Angew. Chem., Int. Ed.* **2012**, *51*, 8762–8767.

(31) Li, J.; Lewis, R. B.; Dahn, J. R. Sodium Carboxymethyl Cellulose: A Potential Binder for Si Negative Electrodes for Li-Ion Batteries. *Electrochem. Solid-State Lett.* **2007**, *10*, A17–A20.

(32) Kovalenko, I.; et al. A Major Constituent of Brown Algae for Use in High-Capacity Li-Ion Batteries. *Science* **2011**, *334*, 75–79.

(33) Choi, S.; Kwon, T.; Coskun, A.; Choi, J. W. Highly elastic binders integrating polyrotaxanes for silicon microparticle anodes in lithium ion batteries. *Science (Washington, DC, U. S.)* **2017**, *357*, 279–283.

(34) Li, X.; Bohn, P. W. Metal-assisted chemical etching in HF/H₂O₂ produces porous silicon. *Appl. Phys. Lett.* **2000**, *77*, 2572–2574.

(35) Huang, Z.; Geyer, N.; Werner, P.; De Boor, J.; Gösele, U. Metal-assisted chemical etching of silicon: A review. *Adv. Mater.* **2011**, *23*, 285–308.

(36) Lee, S. W.; McDowell, M. T.; Berla, L. A.; Nix, W. D.; Cui, Y. Fracture of crystalline silicon nanopillars during electrochemical lithium insertion. *Proc. Natl. Acad. Sci. U. S. A.* **2012**, *109*, 4080–4085.

(37) Liu, X. H.; et al. Size-dependent fracture of silicon nanoparticles during lithiation. *ACS Nano* **2012**, *6*, 1522–1531.

(38) Qian, C.; et al. Non-wettable, oxidation-stable, brightly luminescent, perfluorodecyl-capped silicon nanocrystal film. *J. Am. Chem. Soc.* **2014**, *136*, 15849–15852.

(39) Yang, Z.; Iqbal, M.; Dobbie, A. R.; Veinot, J. G. C. Surface-Induced Alkene Oligomerization: Does Thermal Hydrosilylation Really Lead to Monolayer Protected Silicon Nanocrystals? *J. Am. Chem. Soc.* **2013**, *135* (46), 17595–17601.

(40) Smith, A. J.; Burns, J. C.; Trussler, S.; Dahn, J. R. Precision Measurements of the Coulombic Efficiency of Lithium-Ion Batteries and of Electrode Materials for Lithium-Ion Batteries. *J. Electrochem. Soc.* **2010**, *157*, A196.

(41) Barone, V.; et al. Role and effective treatment of dispersive forces in materials: Polyethylene and graphite crystals as test cases. *J. Comput. Chem.* **2009**, *30*, 934–939.

(42) Giannozzi, P.; et al. Quantum ESPRESSO: a modular and open-source software project for quantum simulations of materials. *J. Phys.: Condens. Matter* **2009**, *21*, 395502.

(43) De Gennes, P. G. Wetting: Statics and dynamics. *Rev. Mod. Phys.* **1985**, *57*, 827–863.

(44) Dalvi, V. H.; Rosky, P. J. Molecular origins of fluorocarbon hydrophobicity. *Proc. Natl. Acad. Sci. U. S. A.* **2010**, *107*, 13603–13607.

(45) Longster, G. F.; Walker, E. E. Effect of permanent dipoles on the cohesive energy and solvent action of some highly polar substances. *Trans. Faraday Soc.* **1953**, *49*, 228–233.

(46) Huang, J. Y.; et al. In Situ Observation of the Electrochemical Lithiation of a Single SnO₂ Nanowire Electrode. *Science* **2010**, *330*, 1515–1520.

(47) McDowell, M. T.; et al. In situ TEM of two-phase lithiation of amorphous silicon nanospheres. *Nano Lett.* **2013**, *13*, 758–764.